

## Antimony based Perovskite Materials for Photovoltaic Applications

Karunakara Moorthy Boopathi, Anupriya Singh, Priyadharsini Karuppuswamy and Chih-Wei Chu\*

Research Center for Applied Sciences, Academia Sinica, Taipei 115, Taiwan

Phone: +886-2-2787-3183 \*E-mail: gchu@gate.sinica.edu.tw

### Abstract

**Organic – inorganic metal halide perovskites have recently emerged as top competitor to be used in solution processable photovoltaic devices as light absorbing material. Here, we report the synthesis of antimony (Sb) based hybrid perovskites have the crystal structure of  $A_3Sb_2I_9$  ( $A = CH_3NH_3$ ,  $CH(NH_2)_2$ ,  $Cs$ ) and investigate their potential in photovoltaic applications. Sb-based perovskite materials showed good absorbance properties; and measured band gap of  $MA_3Sb_2I_9$ ,  $FA_3Sb_2I_9$  and  $Cs_3Sb_2I_9$  were 2.2, 2.3 and 2.3 eV, respectively. The power conversion efficiency of 1.11% was achieved by  $MA_3Sb_2I_9$  perovskite device, which is the highest reported efficiency so far for Sb-based perovskite solar cells.**

### 1. Introduction

Solar energy is the most promising renewable energy technologies to replace conventional energy sources. The recent development of organic – inorganic halide perovskite materials as light harvesting materials in solid state sensitized solar cells has reports record efficiency value of up to 20 % [1, 2]. Especially, methylammonium lead triiodide ( $CH_3NH_3PbI_3$ ) perovskites exhibits very high charge carrier diffusion lengths (particularly for the mixed halide with Cl, up to  $> 1 \mu m$ ) and low exciton binding energy ( $< 50 meV$ ), while having very high absorption coefficient and charge carrier mobility [3, 4]. However, the major disadvantage of the  $CH_3NH_3PbI_3$  is that it contains lead (Pb), which limits the commercialization of this perovskite material due to its toxicity. The most feasible replacements for Pb in  $MAPbI_3$  perovskite structure are the same group 14 metals, such as Sn [5–9] and Ge [10]. However, it was noticed that these compounds can be easily oxidized, which allow quick degradation of tin perovskite compare than lead based perovskite. Hybrid perovskites based on trivalent Sb and Bi are also expected to exhibit semiconducting behavior and very similar band structures to those of divalent Sn- and Pb-based compounds. The perovskite with a structure of  $A_3B_2X_9$  showed reasonable photovoltaic performance and stability while using trivalent Bi metal [11]. Another group 15 element is Sb, which is used widely before in photovoltaic application with chalcogenides ( $Sb_2S_3$ ,  $Sb_2Se_3$ ), achieved PCE of 6.6% [12].

Here, we report antimony based organometal halide perovskite materials have the crystal structure of  $A_3Sb_2I_9$  for lead free inverted planar perovskite solar cells. In this work methylammonium ( $MA^+$ ), formamidinium ( $FA^+$ ) or Cesium ( $Cs^+$ ) have been used as different cation in perovskite structure. The  $A_3Sb_2I_9$  material consists of bioctahedral  $(Sb_2I_9)^{3-}$

clusters that are surrounded by  $MA^+$  (or  $FA^+$  or  $Cs^+$ ) cations. ( $CH_3NH_3$ ) $_3Sb_2I_9$  showed best PCE of 1.11 % under AM1.5G sun illumination.

### 2. Results and Discussion

Different precursors molar ratio of  $SbI_3$  and MAI or FAI or CsI mixed solution were prepared and thin film of those materials were analyzed by UV visible absorption spectroscopy (Fig. 1a). We use a single precursor solution to spin-coat onto substrates; the perovskite then forms upon heating. The peak around 480 nm may confirms the formation of perovskite structure in all three cases and which is not appeared in  $SbI_3$  thin film. The optical bandgap calculated from UV-visible absorption spectra and Tauc plot of  $SbI_3$ ,  $MA_3Sb_2I_9$ ,  $FA_3Sb_2I_9$  and  $Cs_3Sb_2I_9$  were 2.6, 2.2, 2.3 and 2.3 eV, respectively (Fig. 1b). Photoemission spectroscopy in air (PESA) used to measure the valence band (VB) of  $SbI_3$ ,  $MA_3Sb_2I_9$ ,  $FA_3Sb_2I_9$  and  $Cs_3Sb_2I_9$  perovskites showed 5.86, 5.48, 5.5 and 5.3 eV, respectively (Fig. 1c), and from the observed optical bandgap values, the conduction bands (CBs) are calculated to be 3.26, 3.28, 3.2 and 3 eV, respectively, as shown in Fig. 1d.

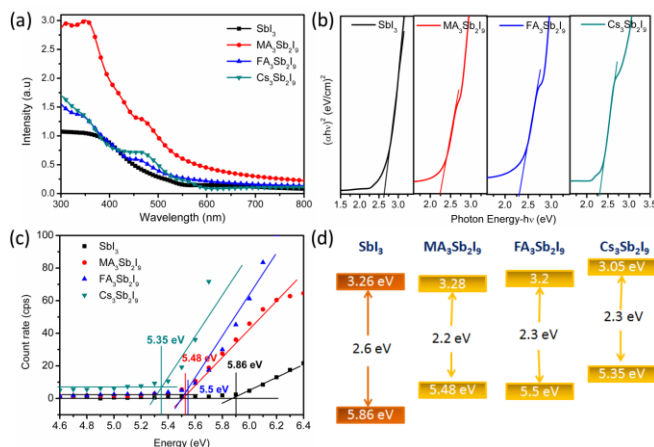


Fig 1 a) Optical absorption spectra, (b) Tauc plot, (c) PESA and (d) Schematic energy band diagram of  $SbI_3$ ,  $MA_3Sb_2I_9$ ,  $FA_3Sb_2I_9$  and  $Cs_3Sb_2I_9$  thin films.

From the energy band diagram, it clearly shows that there is feasibility of enhancing device performance by manipulating hybrid donor– acceptor materials with different energy levels. Bandgap of their materials proves that it can be used for solar cells and also good materials for other optoelectronics applications.

Topography of  $MA_3Sb_2I_9$  imaged by scanning electron microscopy shows the hexagonal thin sheet structure with uni-

form in size and almost covered completely on PEDOT:PSS surface (Fig.2 a,b). Very few voids appear between the crystals in the MA<sub>3</sub>Sb<sub>2</sub>I<sub>9</sub> films. In case of FA<sub>3</sub>Sb<sub>2</sub>I<sub>9</sub>, perovskite film was not continuous and lot pin holes were appeared (Fig. 2 c,d). Smaller crystallite grains and non-uniform in size were observed, which is not beneficial for photovoltaic applications. Cs<sub>3</sub>Sb<sub>2</sub>I<sub>9</sub> showed non continuous perovskite film with two different contract presents on surface. It may due to presence of unreacted CsI or SbI<sub>3</sub> during the formation of perovskite structure upon annealing (Fig. 3 e,f). MA<sub>3</sub>Sb<sub>2</sub>I<sub>9</sub> and Cs<sub>3</sub>Sb<sub>2</sub>I<sub>9</sub> shows relatively smooth and better morphology while comparing than FA<sub>3</sub>Sb<sub>2</sub>I<sub>9</sub>. Formation of pores depends upon the interaction energies of the perovskite and air, and the perovskite and the substrate.

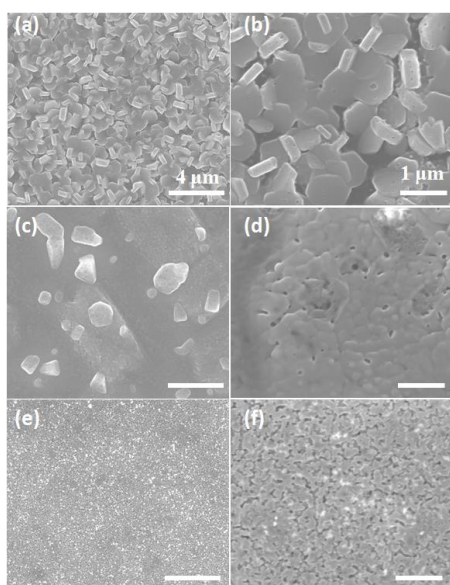


Fig. 2 SEM image of (a, b) MA<sub>3</sub>Sb<sub>2</sub>I<sub>9</sub>, (c, d) FA<sub>3</sub>Sb<sub>2</sub>I<sub>9</sub> and (e, f) Cs<sub>3</sub>Sb<sub>2</sub>I<sub>9</sub> at optimized molar ratio; (a, c, e) lower magnification and (b, d, f) higher magnification.

We fabricated devices having the architecture glass/ITO/PEDOT:PSS/perovskite/PC71BM/C60/BCP/AI and investigated their PV performance. Here, we used C<sub>60</sub> to minimize the trap densities. Fig. 3a and 3b display photocurrent density– voltage (J–V) and External quantum efficiency (EQE) curves of perovskite solar cells prepared with three different cations (at their optimized molar ratio); Table 1 list the corresponding photovoltaic parameters.

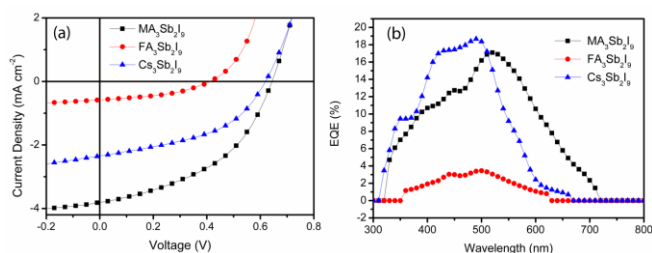


Fig. 3 (a) J–V characteristics and (b) EQE of best perovskite-PC<sub>71</sub>BM planar heterojunction solar devices with different perovskite materials.

Table 1 Photovoltaic performance parameters of devices prepared with different perovskites.

Perovskite	V <sub>oc</sub> (V)	J <sub>sc</sub> (mA cm <sup>-2</sup> )	FF(%)	PCE(%)
MA <sub>3</sub> Sb <sub>2</sub> I <sub>9</sub>	0.64	3.81	45.42	1.11
FA <sub>3</sub> Sb <sub>2</sub> I <sub>9</sub>	0.41	0.58	42.05	0.10
Cs <sub>3</sub> Sb <sub>2</sub> I <sub>9</sub>	0.62	2.34	46.18	0.67

### 3. Conclusions

In summary, we successfully prepared solution processable antimony based perovskite solar cells by single step spin coating method and achieved PCE of 1.11%. Overall, the results of the present study demonstrate the strong potential of Sb-based halide perovskite compounds in optoelectronic devices especially in photovoltaic applications.

### Acknowledgements

Dr. Chu thanks the Ministry of Science and Technology (MOST) of Taiwan (104-2221-E-001-014-MY3) and the Career Development Award of Academia Sinica, Taiwan (103-CDA-M01), for financial support.

### References

- [1] M. Saliba, S. Orlandi, T. Matsui, S. Aghazada, M. Cavazzini, J.-P. Correa-Baena, P. Gao, R. Scopelliti, E. Mosconi, K.-H. Dahmen, F. De Angelis, A. Abate, A. Hagfeldt, G. Pozzi, M. Graetzel and M. K. Nazeeruddin. *Nat. Energy*. **1** (2016) 15017.
- [2] W. S. Yang, J. H. Noh, N. J. Jeon, Y. C. Kim, S. Ryu, J. Seo and S. I. Seok. *Science*. **348** (2015) 1234.
- [3] J. M. Ball, M. M. Lee, A. Hey and H. J. Snaith, *Energy Environ Sci*. **6** (2013) 1739.
- [4] V. Gonzalez-Pedro, E. J. Juarez-Perez, W.-S. Arsyad, E. M. Barea, F. Fabregat-Santiago, I. Mora-Sero and J. Bisquert, *Nano Lett*. **14** (2014) 888.
- [5] F. Hao, C. C. Stoumpos, D. H. Cao, R. P. H. Chang and M. G. Kanatzidis. *Nat Photon*. **8** (2014) 489.
- [6] F. Zuo, S. T. Williams, P.-W. Liang, C.-C. Chueh, C.-Y. Liao and A. K. Y. Jen. *Adv. Mater*. **26** (2014) 6454.
- [7] M. H. Kumar, S. Dharani, W. L. Leong, P. P. Boix, R. R. Prabhakar, T. Baikie, C. Shi, H. Ding, R. Ramesh, M. Asta, M. Graetzel, S. G. Mhaisalkar and N. Mathews. *Adv. Mater*. **26** (2014) 7122.
- [8] S. J. Lee, S. S. Shin, Y. C. Kim, D. Kim, T. K. Ahn, J. H. Noh, J. Seo and S. I. Seok, *J. Am. Chem. Soc*. **138** (2016) 3974.
- [9] L. Serrano-Lujan, N. Espinosa, T. T. Larsen-Olsen, J. Abad, A. Urbina and F. C. Krebs, *Adv. Energy Mater*. **5** (2015) 150119.
- [10] T. Krishnamoorthy, H. Ding, C. Yan, W. L. Leong, T. Baikie, Z. Zhang, M. Sherburne, S. Li, M. Asta, N. Mathews and S. G. Mhaisalkar, *J. Mater. Chem. A*. **3** (2015) 23829.
- [11] B.-W. Park, B. Philippe, X. Zhang, H. Rensmo, G. Boschloo and E. M. J. Johansson, *Adv. Mater*. **27** (2015) 6806.
- [12] Y. C. Choi, Y. H. Lee, S. H. Im, J. H. Noh, T. N. Mandal, W. S. Yang and S. I. Seok, *Adv. Energy Mater*. **4** (2014) 1301680.